RESEARCH ARTICLE

Alkylation of benzene with carbon dioxide to low-carbon aromatic hydrocarbons over bifunctional Zn-Ti/HZSM-5 catalyst

Xiangyu Liu[1], Yanling Pan[2], Peng Zhang[1], Yilin Wang[1], Guohao Xu[1], Zhaojie Su[1], Xuedong Zhu (✉)[1], Fan Yang (✉)[1]

1 Engineering Research Center of Large-Scale Reactor Engineering and Technology, Ministry of Education, East China University of Science and Technology, Shanghai 200237, China
2 Department of Product Engineering, School of Chemical Engineering, East China University of Science and Technology, Shanghai 200237, China

Abstract Alkylation of benzene to value-added, high octane number and low toxic toluene and xylenes provides a way to lower benzene content in gasoline pool, and is hence a method to promote fuel quality. On the other hand, CO_2 accumulation in the atmosphere causes global warming and requires effective route for its valorization. Utilization of CO_2 as a carbon source for benzene alkylation could achieve both goals. Herein, alkylation of benzene with CO_2 and H_2 was realized by a series of low-cost bifunctional catalysts containing zinc/titanium oxides (Zn/Ti oxides) and HZSM-5 molecular sieves in a fixed-bed reactor. By regulating and controlling oxygen vacancies of Zn/Ti oxides and the acidities of HZSM-5, benzene conversion and CO_2 conversion reached 28.7% and 29.9% respectively, along with a total selectivity of toluene and xylene higher than 90%. In this process, more than 25% CO_2 was effectively utilized and incorporated into the target products. Moreover, the mechanism of the reaction was analyzed and the course was simultaneously traced. CO_2 was transformed into methanol firstly, and then methanol reacted with benzene generating toluene and xylene. The innovation provides a new method for upgrading of fuels and upcycling the emissions of CO_2, which is of great environmental and economic benefits.

Keywords carbon dioxide, benzene, alkylation, bifunctional catalyst, mechanism

1 Introduction

Excessive emissions of CO_2 have become one of the main culprits of environmental and climatic problems such as global warming. Therefore, how to make full use of the emissions of CO_2 is of great interest. At present, CO_2 is mainly converted into non-renewable fuels or other chemicals, via various methods like catalytic and electro-chemistry methods [1–3]. Distinct from the abundance of CO_2, toluene and xylene, as indispensable industrial chemicals, are short in supply in many regions. Researchers have been focusing on the conversion of CO_2 into toluene and xylene [4–6], with the challenge wherein low CO_2 conversion and toluene/xylene selectivity are often confronted (Table S1, cf. Electronic Supplementary Material, ESM). Recently, a sharp drop in benzene price has been witnessed owing to a progressively stringent guidelines for its entering into the gasoline pool. If benzene and CO_2 could be co-converted into aromatics such as toluene and xylenes, the aforementioned issues can also be solved simultaneously. Compared with other toluene/ xylene production methods [7–9] and CO_2 conversion methods [10], this route promises more advantages. Thus far, there are relatively few studies or discussions devoted to the alkylation of benzene with CO_2 and H_2 (ABCH reaction).

A bifunctional catalyst is considered for ABCH reaction, one active site of the catalyst provides a chance to transform CO_2 and H_2 into an intermediate and the intermediate reacts with benzene on the other active site. In former studies involving conversion of CO_2 into aromatics, methanol was determined to be a key intermediate in many circumstances [4,5,9]. Therefore, integrating methanol synthesis from CO_2 and benzene alkylation to

produce catalyst in ABCH reaction is reasonable. In a previous report, rhenium supported on TiO_2 was coupled with zeolites and used to catalyze the ABCH reaction in a continuous stirred tank reactor (CSTR), over which a toluene yield of 36% was obtained [11]. However, cost-sensitive rhenium and the discontinuous CSTR restrict the largescale applications, thus low-cost catalyst and easy-use reactors are in need. The oxygen vacancies (OVs) of TiO_2 acted as adsorption sites for CO_2, and the catalytic activity of TiO_2 was modified by doping with other metal oxides aside from rhenium [12,13], among which ZnO as active site for H_2 hetero-dissociation revealed to be the most promising one in methanol synthesis from CO_2 [4,5,14]. As acid sites of zeolite are capable of catalyzing alkylation reaction between methanol and benzene, mixing proper zeolites such as ZSM-5 with synthesized metal oxides to generate a bifunctional catalyst is considered to be feasible for ABCH reaction, still, the relevant reports are insufficient. In addition, for the catalysts used in ABCH reaction, the true active sites and the structure-performance relationship remain unclear.

In this study, a series of low-cost bifunctional catalysts containing ZnO/TiO_2 oxides and HZSM-5 molecular sieves have been successfully prepared. The compositions of catalysts were manipulated with respect to the elements ratios of metal oxides and Si/Al ratios in HZSM-5 zeolites. The characteristics of these catalysts were extensive characterized using a panoply of techniques. The corresponding reaction mechanism, especially the activation of CO_2 and its further conversions, was monitored by *in-situ* infra-red (*in-situ* IR) spectroscopy, in order to better understand the process. These findings provide useful ideas and techniques for developing new and more effective catalysts used in ABCH reactions.

2 Experimental

2.1 Chemical reagents and materials

Zinc nitrate hexahydrate (AR) was provided by General-Reagent company. Titanium (IV) oxysulfate-sulfuric acid hydrate (AR), cetyl-trimethyl ammonium bromide (CTAB, AR), sodium hydroxide (AR), sulfuric acid (AR, 99.8 wt-%), and benzene (AR) were provided by Aladdin company. HZSM-5 (Si/Al = 13.5, 30, 100) were purchased from Nankai University Catalyst Plant. Mixed gas containing CO_2, H_2 and nitrogen (N_2) were purchased from Air Liquide (China) Investment Co. LTD. All the reagents were utilized directly without further purification.

2.2 Preparation of catalysts

2.2.1 Preparation of active components

TiO_2 and Zn/Ti oxides were prepared by hydrothermal method. Typically, a certain amount of titanium oxysulfate was dissolved in a beaker containing a small amount of concentrated sulfuric acid (5 mL) in ultrafine water (150 mL) at room temperature. The obtained mixture was stirred for 24 h, followed by adding designated amount of zinc nitrate hexahydrate. Next, the solution was added into another beaker containing CTAB solution at a rate of 1 drop per second. Subsequently, pH of the mixture was adjusted to around 10 by 1.0 mol/L NaOH solution. The product was further stirred for an additional 2 h before transferred to a Teflon-lined autoclave to proceed hydro-thermal synthesis at 473 K for 20 h. The final product was collected through centrifugation, washed with water. The obtained samples were dried in a vacuum oven at 363 K for 12 h, calcined in a muffle furnace at 773 K for 4 h (temperature was elevated at ramp of 5 K/min) to acquire Zn/Ti oxides. The oxides with different Zn/Ti molar ratios were named Zn_xTi, wherein x means the molar ratios of Zn/Ti. The preparation process of oxidized zinc was identical to the above synthesis method except that sulfuric acid and titanium sulfate are not required.

2.2.2 Preparation of tandem catalyst

Physical mixing method was adopted for the preparation of the tandem catalyst, which was shown to enhance catalytic activity compared with other mixing methods [9]. Zn/Ti oxides and HZSM-5 zeolite with various Si/Al ratios were grounded at the mass ratio of 1:1. The metal oxides and zeolite mixture were pelleted into particles (20−40 mesh), and calcined in a muffle furnace for 5 h at 773 K. The mixtures were denoted as Zn_xTi-HZ5 (y) ("y" refers to the Si/Al ratio of HZSM-5).

2.3 Characterizations

The surface compositions and chemical states of all samples were measured and recorded by Thermo Escalab 250 for X-ray photoelectron spectroscopy (XPS), operating at 1486.6 eV monochromatic Al Kα source as well as 14 kV and 30 mA. The standard binding energy of C1s peak of adventitious carbon contamination was adopted at 284.8 eV. The XPS original data was deconvoluted using the Peak4.1 software via Gaussian-Lorentzian method.

X-ray powder diffraction (XRD) patterns were measured on a D/max2550VB/PC Rotating Anode X-ray Powder Diffractometer, with the Cu Kα (18 kW, 450 mA) as the source of radiation, at the ramp of 8°/min and the step size of 0.02°. The scanning range and angle measuring accuracy of this instrument were 5°–80° and $\Delta 2\theta \leqslant 0.02°$, respectively.

Temperature-programmed desorption of ammonia (NH_3-TPD) was measured on Chemisorb™2920 manufactured by Micromeritics. The catalyst sample was first heated to 873 K at 10 K/min, in helium for 1 h. 10% NH_3 in helium was fed into the samples for saturation after the sample was cooled to room temperature. Then samples

were heated to 453 K in helium to remove the physically adsorbed NH_3. Desorption was carried out at the ramp of 10 K/min up to 993 K, meanwhile the thermal conductivity detector signal was recorded.

The concentration and proportion of elements were quantitatively determined by inductively coupled plasma atomic emission spectrometer (ICP-AES) manufactured in Agilent, USA.

The surface morphology and particle size analysis of the samples were obtained by a GeminiSEM 500 field-emission scanning electron microcopy (FE-SEM). Platinum plating of the instrument was constructed before testing the sample.

Electron paramagnetic resonance (EPR) was measured with Emx-8/2.7 electro-spin resonance spectrometer of Broker (the U.S.), which detects free radicals, transition metals, oxygen defects and other information of the samples.

In-situ IR spectroscopy was performed to discover the catalytic mechanism of the procedure. The spectra were recorded by ThermoFisher Nicolet iS50 equipped with a deuterated triglycine sulfate detector. The absorbance was obtained by collecting 32 scans at 4 cm^{-1} resolution.

To ameliorate the different degrees of light absorption and light scattering, Raman spectrum of laser sources with different wavelengths was used to detect the phases at different depths [15], whereby, the surface and bulk phase structures of the catalysts were detected at 325 and 785 nm.

2.4 Catalytic evaluation

ABCH reaction was completed in a fixed bed reactor employing a 316 stainless-steel tube. The catalyst (1 g) was put into the constant temperature area of the stainless-steel tube, and the rest of the tube was filled with quartz. The molar ratio of $H_2:CO_2:C_6H_6$ in whole feed was estimated about 12:4:1. Before the reaction, catalysts were reduced at 698 K in H_2 for 1 h. After reduction, reaction gas ($H_2:CO_2$ = 3:1) was fed into the reactor at 150 mL/min under the control of mass flowmeter and benzene at 0.03 mL/min was also pumped in. The pressure of the system was kept at 3.0 ± 0.02 MPa via a back-pressure valve and temperature was kept at 698 K $\pm$ 3 K via a temperature controller. Agilent 8890 GC provided online real-time analysis for gaseous state products every two hours, and gave offline detection of liquid state products when cooling down. The conversion of benzene, and the selectivity of toluene and xylene or other aromatics were used as the indexes to evaluate the reaction performance. The calculation formula is as follows:

$$Conv(benzene)mol\text{-}\%$$
$$= \frac{benzene\ in\ feed - benzene\ in\ liquid\ product}{benzene\ in\ feed}$$
$$\times 100\%, \tag{1}$$

$$Select(i)mol\text{-}\%$$
$$= \frac{i\ in\ liquid\ product - i\ in\ feed}{benzene\ in\ feed - benzene\ in\ liquid\ product}$$
$$\times 100\%, \tag{2}$$

where i are toluene, xylene and other aromatics.

3 Results and discussion

3.1 Characterization of metal oxides and coupling catalysts

Figure 1 shows the XRD pattern of TiO_2 samples with various Zn contents. It implies that Zn doping influenced the morphology of TiO_2 obviously. Without the incorporation of zinc, TiO_2 displayed typical brookite structure (PDF#76-1935), showing peaks at 25.2°, 26.0° and 31.0°, etc. When a large quantity of TiO_2 was transformed into anatase (PDF#73-1764), immediately was incorporated by a small amount of ZnO (Zn/Ti = 0.01). The peaks at 25.8°, 36.4° and 37.5° disappeared, afterwards they were replaced by peaks at 25.4°, 38.0° and 62.8°, respectively. Anatase was observed to be the only phase if Zn/Ti = 0.1. With further increasing the amount of Zn, such as Zn/Ti = 0.3 and Zn/Ti = 0.5, the characteristic peaks of the anatase phase became weaker and ZnO phase ($2\theta = 35.3°, 62.8°$) gradually became highlighted. Continuously adding Zn ($Zn_{1.0}Ti$), peaks at 56.7°, 35.4° and 32.5° then emerged, indicating the formation of $Zn_2Ti_3O_8$ [16–18]. As a whole, the addition of Zn element led to the phase of TiO_2 change from brookite to anatase structure or $Zn_2Ti_3O_8$, and the excess zinc exists in the form of ZnO.

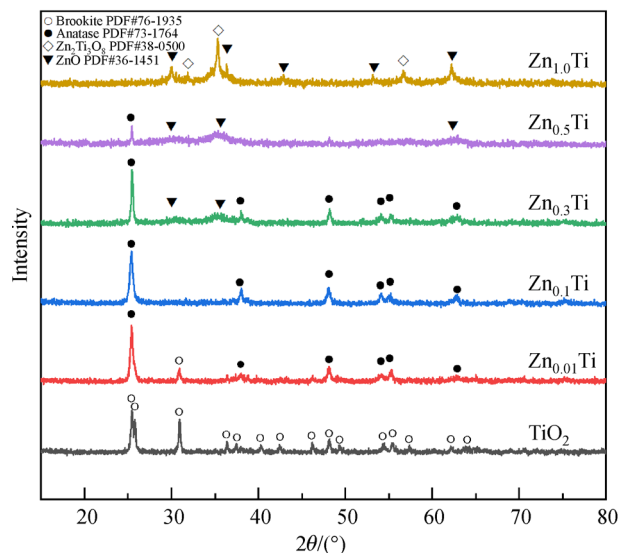The chemical states of compositional elements were

Fig. 1 XRD patterns of metal oxides with the different zinc contents.
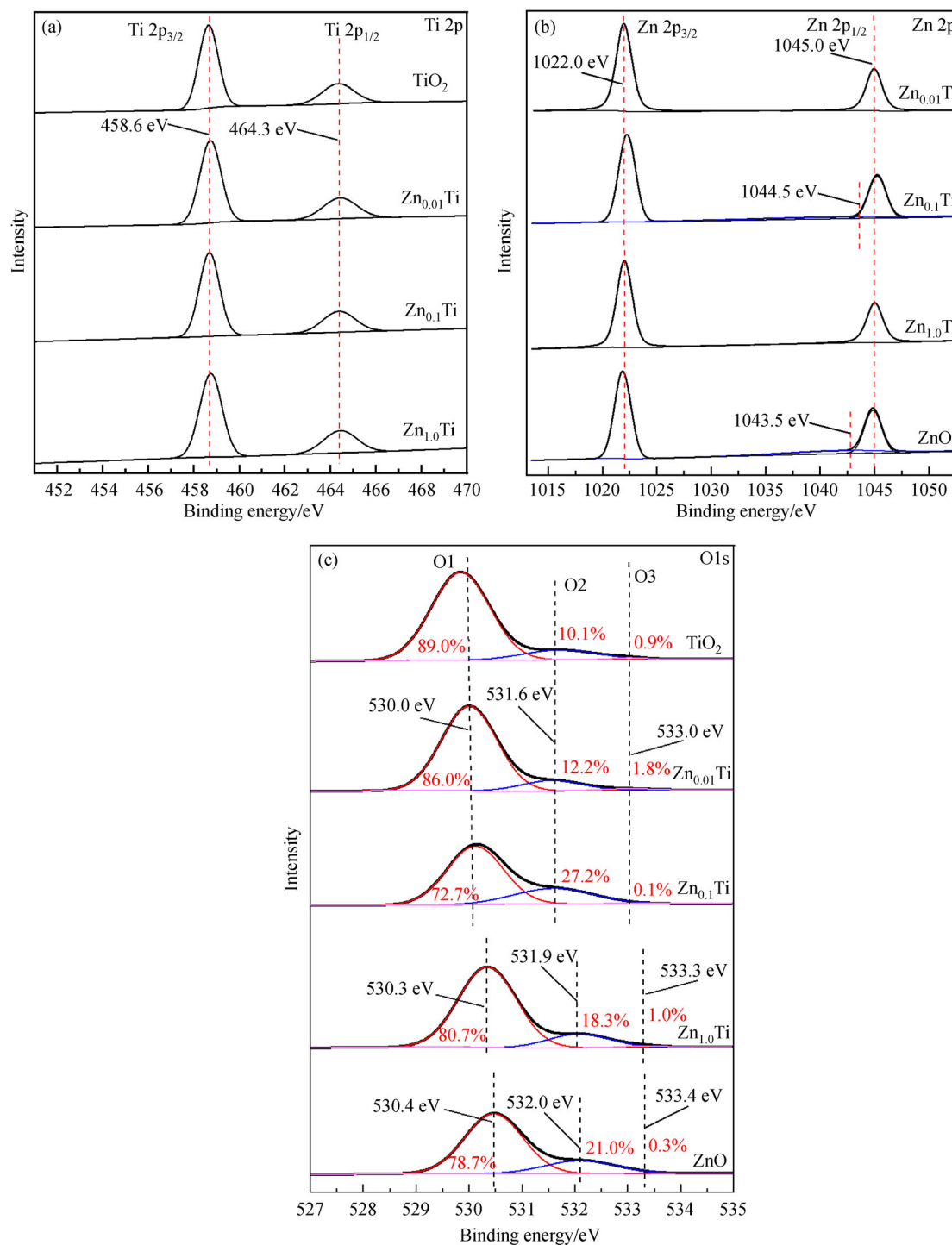
**Fig. 2** XPS spectrums of (a) Ti 2p; (b) Zn 2p; (c) O 1s orbitals.

inspected by XPS as depicted in Fig. 2. Ti 2p XPS peaks at 458.6 and 464.3 eV [19,20] were rather symmetrical without any shoulder peaks for Ti^{2+} or Ti^{3+} located between 456–457 eV [19–22], indicating Ti in most samples exists as Ti^{4+}. In addition, this also means that the introduction of Zn did not affect the binding energies (BEs) of Ti. Figure 2(b) shows the Zn 2p XPS spectra, in all samples the spin-orbit split 2p1/2 and 2p3/2 peaks were observed at about 1045 and 1021 eV, respectively [23,24]. There is no obvious difference of peak positions in Fig. 2(b). Meanwhile, a small and broad shoulder appears at the lower BEs, as observed in ZnO (1043.5 eV) and $Zn_{0.1}Ti$ (1044.5 eV), which was due to the occurrence of metal vacancies [25].

The XPS spectrum of O1s is illustrated in Fig. 2(c). Three peaks appear around 530.0, 531.6 and 533.0 eV, corresponding to O1, O2 and O3 species respectively. The appearance of the O1 species near 530.0 eV was attributed to lattice oxygen in ZnO and TiO_2 lattice [26]. O1 indicated that oxygen from metal oxide lattice in the state of O^{2-} occupied the majority of the surface oxygen. The acromion of O2 species (near 531.6 eV) and O3 species (near 533.0 eV) were attributed to the presence of lower-charged oxygen ions (surface −OH) and chemisorbed oxygen, both resulting from the OVs on the oxide surface [21,26,27]. Moreover, the sample doped with 10% Zn possessed the highest oxygen vacancy (OV) content (up to about 27.2%). Notably, the XPS peaks of oxygen were gradually shifted to higher BEs with the increase of Zn content. This phenomenon possibly stemmed from the high electronegativity of Zn (compared to Ti), which weakened the constraint exerted on its electrons from oxygen nuclear [28–30].

OVs are generally believed to be the active sites for CO_2 conversion [31,32]. In this study, OVs were further measured by EPR then EPR signals responded to unpaired electrons in oxygen defects, and the results are shown in Fig. 3. Significant changes of signal value were observed in neither TiO_2 nor $Zn_{0.01}Ti$, while those signals of $Zn_{0.1}Ti$, $Zn_{1.0}Ti$, and ZnO appeared at $g = 1.993$, indicating the existence of OVs [33]. Moreover, $Zn_{0.1}Ti$ samples possessed the largest content of OVs, which was consistent with the XPS results.

The texture properties were studied via SEM and nitrogen adsorption-desorption. The SEM micrographs are displayed in Fig. 4. HZSM-5 shows a coffin-like shape, with inerratic particle size (about 2 μm) and smooth surface. For tandem catalysts consisting of both metal oxides and HZSM-5, the metal oxides in irregular forms were attached to the surfaces of HZSM-5 or aggregated with each other. Nitrogen adsorption-desorption data of catalyst samples are summarized in Table 1. Pure TiO_2 shows a BET surface area of 22 m^2/g, which increased with
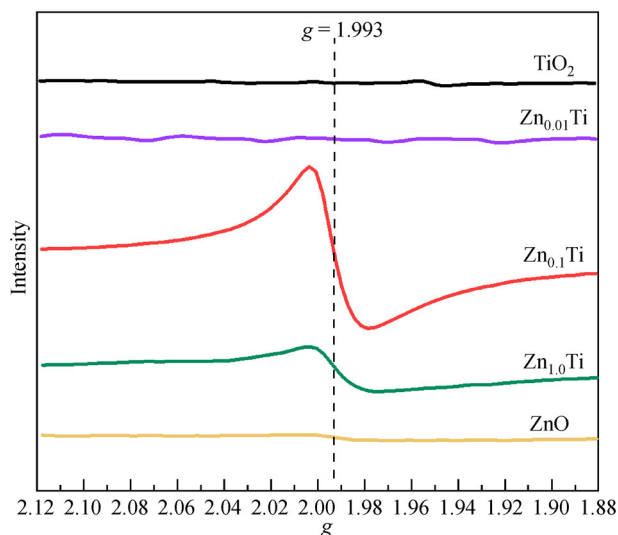
Fig. 3 EPR spectrums of several metal oxides with the different zinc contents.

the addition of Zn, reaching the maximum at 151 m^2/g when Zn/Ti = 0.5, then the surface area gradually dropped to 40 m^2/g for ZnO. The surface area of mixed Zn_xTi-HZ5 catalysts showed a similar changing trend with that of metal oxides.

In addition, ICP-AES and XPS were used to analyze the bulk and surface compositions of mental oxides. $Zn_{1.0}Ti$ showed a similar Zn/Ti ratio in surface and bulk, yet the surface Zn/Ti ratios of other samples were significantly higher than those of the bulk, indicating that the surface was enriched with Zn. This difference was attributed to the morphologies as described in XRD results, further testifying that the interaction between Zn and Ti changed with their relative compositions.

In order to further explore the reasons for this phenomenon, Raman spectroscopy was used to characterize the phase structure and Fig. 5 shows the results. As for the pure TiO_2, Raman peaks of two wavelengths typically

Table 1 Nitrogen adsorption and desorption results and Zn/Ti ratios of different samples

Sample	A_{BET1} /(m²·g⁻¹)	V_{pore} /(mL·g⁻¹)	D_{pore} [a] /nm	Zn/Ti ratio [b] Surface	Zn/Ti ratio [b] Bulk	Sample	A_{BET2} /(m²·g⁻¹)	V_{pore} /(mL·g⁻¹)	D_{pore} [a] /nm	ΔA [c] /(m²·g⁻¹)
TiO_2	22	0.16	3.98	0	0	TiO_2-HZ5	180	0.23	1.82	158
$Zn_{0.01}Ti$	45	0.20	3.81	0.04	0.01	$Zn_{0.01}Ti$-HZ5	183	0.29	1.82	138
$Zn_{0.1}Ti$	63	0.33	2.91	0.25	0.11	$Zn_{0.1}Ti$-HZ5	184	0.29	1.84	121
$Zn_{0.3}Ti$	104	0.24	5.75	n.d[d]	0.34	$Zn_{0.3}Ti$-HZ5	225	0.33	1.82	121
$Zn_{0.5}Ti$	151	0.30	5.02	n.d[d]	0.54	$Zn_{0.5}Ti$-HZ5	244	0.29	1.83	93
$Zn_{1.0}Ti$	115	0.28	5.04	0.96	1.05	$Zn_{1.0}Ti$-HZ5	202	0.27	1.82	87
ZnO	40	0.02	8.02	∞	∞	ZnO-HZ5	142	0.14	1.84	102
γ-Al_2O_3	176	0.31	2.65	n.d[d]	n.d[d]	HZSM-5	313	0.14	1.84	n.d[d]

a) Diameter of most holes by BJH method; b) surface: Zn/Ti ratio measured by XPS, bulk: Zn/Ti ratio measured by ICP-AES; c) approximation of specific surface area of HZ5 not covered by oxide: $\Delta A = A_{BET2} - A_{BET1}$; HZ5 means HZSM-5; d) None tests taken.
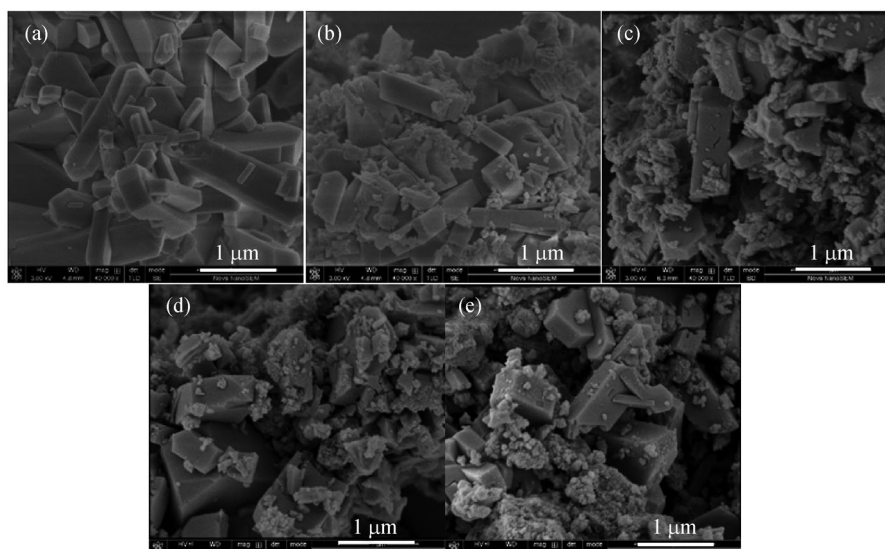
Fig. 4   SEM patterns of several catalysts: (a) HZSM-5(30), (b) TiO_2-HZ5(30), (c) $Zn_{0.01}Ti$-HZ5(30), (d) $Zn_{0.1}Ti$-HZ5(30), and (e) $Zn_{1.0}Ti$-HZ5(30).
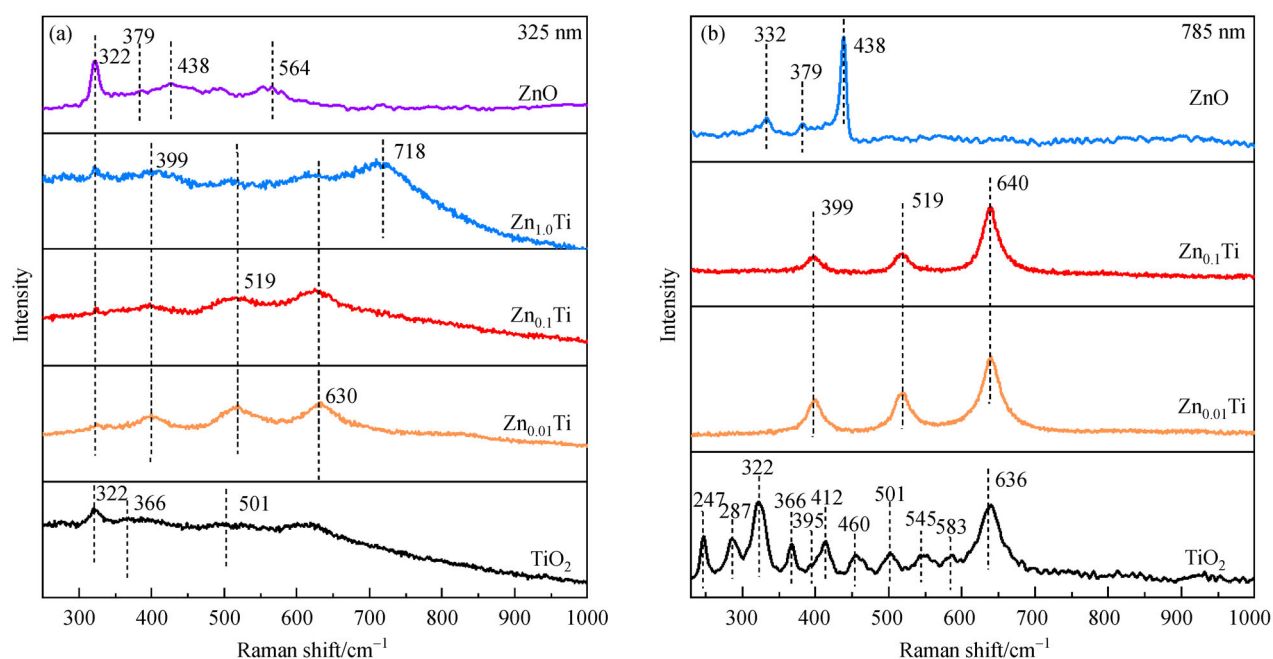
Fig. 5   Raman spectroscopies of several metal oxides with the different zinc contents used different laser sources: (a) 325 nm and (b) 785 nm.

rose from brookite crystal phase, which was appropriately allocated to the modes of A_{1g} (247, 412 and 636 cm^{-1}), B_{1g} (322 and 501 cm^{-1}), B_{2g} (366, 395, 460 and 583 cm^{-1}) and B_{3g} (287 and 545 cm^{-1}), respectively [34]. But for $Zn_{0.01}Ti$ and $Zn_{0.1}Ti$, Raman peaks of brookite disappear, substituted by the anatase characteristic peaks. In $Zn_{0.01}Ti$ and $Zn_{0.1}Ti$, for the wavelength of 325 nm, peaks at 399 cm^{-1} [B_{1g}], 519 cm^{-1} [B_{1g}], and 630 cm^{-1} [E_g] were observed, while for the wavelength of 785 nm, peaks at 399 cm^{-1} [B_{1g}], 519 cm^{-1} [B_{1g}] and 640 cm^{-1} [E_g] were observed, among which [B_{1g}] and [E_g] were attributed to the partial

modes of six Raman active modes peaks of anatase TiO_2 [35–37]. It should be emphasized, the characteristic peak at 322 cm^{-1} [E_2 phonon mode] using 325 nm standing for ZnO was also observed in $Zn_{1.0}Ti$, $Zn_{0.1}Ti$ and $Zn_{0.01}Ti$, but the peak at 332 cm^{-1} using 785 nm found in ZnO was not detected in other samples [15,16,38,39]. This demonstrates there were several ZnO phase on the surface of Zn/Ti oxides rather than in the bulk. That exactly agrees with the results of ICP-AES and XPS in Table 1. In contrast, the surface layer of $Zn_{1.0}Ti$ sample was composed of three crystal types (322 cm^{-1} owing to ZnO [16]; 399, 519 and

630 cm^{-1} due to anatase [35–37]; 718 cm^{-1} [A$_{1g}$ phonon mode] was attributed to Zn$_2$Ti$_3$O$_8$ [16]), which revealed that the surface Zn/Ti ratio of Zn$_{1.0}$Ti sample was distinct from others.
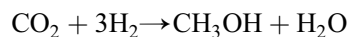
The acidities were examined by NH$_3$-TPD. As revealed in Fig. 6, two peaks were seen between 100 K and 773 K, denoting to NH$_3$ desorbed on weak and strong acid sites of HZSM-5. Compared with HZSM-5(30), the introduction of metal oxide weakened the total acidity, especially for the strong acid sites. The total acidity dropped drastically with the increase of Zn loading, due to the coverage of acid sites within HZSM-5 by metal oxides [40,41]. Simultaneously, metal oxides also weakened the strength of the strong acid sites (the peak reduces from 644 K to about 598 K) and enhanced the strength of the weak acid sites (the peak heightens from 459 K to around 473 K). Moreover, Si/Al ratios showed significant effects on the acidities, in which catalyst with a lower Si/Al ratio possessed a higher acidity.

3.2 Catalytic evaluation

3.2.1 Determination of reaction conditions

For alkylation of benzene with syngas, many studies have shown that the reaction was the coupling of synthesis gas to methanol and the alkylation of benzene with methanol. As mentioned above, in previous studies, ABCH reaction was regarded as a tandem reaction composed of methanol synthesis via CO$_2$/H$_2$ and alkylation of benzene with methanol, which was similar with what happened in alkylation of benzene with syngas [9,27,42]. In the first step, low temperature was conducive for CO$_2$/H$_2$ to form methanol owing to thermodynamic reasons (Eqs. (1) and (2), Fig. S1, cf. ESM) [43,44]. Nonetheless, the reaction of

Fig. 6 NH$_3$-TPD patterns of catalysts with different Zn/Ti and Si/Al ratios.

reverse water gas shift (RWGS) dominates under high temperatures and CO becomes the main products.

$$CO_2 + 3H_2 \rightarrow CH_3OH + H_2O$$

$$\Delta H_{298K} = -49.5\,kJ/mol \qquad (1)$$

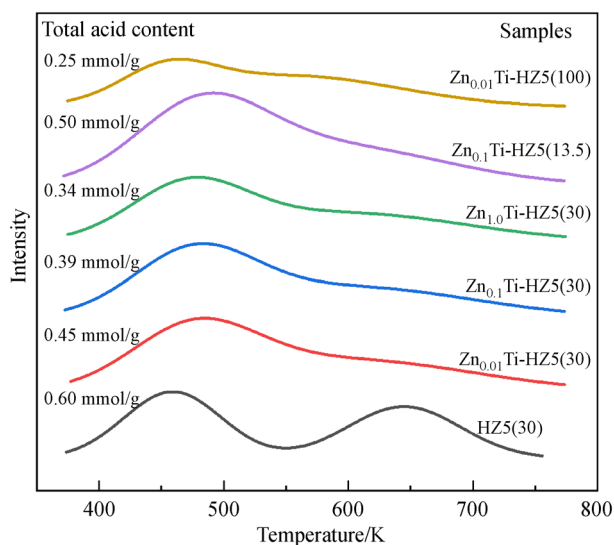$$CO_2 + H_2 \rightarrow CO + H_2O \quad \Delta H_{298K} = +41.2\,kJ/mol \quad (2)$$

On the contrary, alkylation of benzene was carried out at comparable higher temperatures [9,26,45,46]. However, conditions benefiting benzene conversion are detrimental for methanol synthesis. As a balance between benzene conversion and CO selectivity, the optimal reaction conditions were suggested to be: 698 K, 3 MPa, H$_2$:CO$_2$ = 3:1, gas hourly space velocity (GHSV) = 9000 h^{-1}, liquid hourly space velocity (LHSV) = 1.8 h^{-1} (Figs. S2–S5, Table S2, cf. ESM) via a series of experiments.

3.2.2 Effects of metal oxides

Table 2 shows the distribution and selectivity of liquid products, clearly, benzene could hardly be converted in the absence of Zn. Benzene conversions displayed a "volcano-type" trend as Zn content grew, it climbed from 1.1% to 23.8%, then dropped to 13.5%, when Zn/Ti was zero, 0.1 and ∞, respectively. As for the selectivity, toluene made up the majority of the products with the selectivity within 77.4%–88.5% and xylenes were the second-largest product, accounting for 4.7%–18.2% of the products. Ethylbenzene and C$_{9+}$ were the main side products in the liquid phase, accounting for less than 10% in most samples. Para-xylene (PX) constituted about 25% in all xylenes, which was a thermal equilibrium composition. Generally, xylene selectivity showed the same tendency as that of benzene conversion, while the toluene selectivity changed oppositely.

Besides, the parameter 'phenyl ring efficiency' was especially introduced (Table 2) to represent the utilization efficiency of phenyl rings from benzene. The results indicated that a high phenyl ring utilization rate (more than 95%) could be obtained in all tests, which means the phenyl rings of benzene are successfully utilized in the alkylation process, side reactions like over hydrogenation of benzene and thermal cracking were largely avoided.

Table 3 shows the evaluation results of the gas phase products. CO$_2$ conversion was basically maintained at 20%−30% and gradually increased with the introduction of Zn, which was because Zn promoted the activation of hydrogen and the activated hydrogen facilitated the conversion of CO$_2$ [14,31,33,43]. Carbon monoxide, methane, and a small number of C$_2$–C$_4$ hydrocarbons were the primary components, while methanol or dimethyl ether were not observed. Apparently, CO selectivity rose and methane selectivity declined with Zn addition, which

Table 2 Distribution and selectivity of liquid alkylation products of catalysts with different Zn/Ti ratios [a]

Catalyst	Conversion/%	Selectivity/%						Phenyl ring yield [b] /%
	Benzene	Toluene	Xylene	EBZ [c]	C_{9+}	PX/X [d]	
TiO_2-HZ5(30)	1.1	86.0	6.8	4.5	2.7	24.4	99.8
$Zn_{0.01}Ti$-HZ5(30)	8.4	88.5	6.7	2.7	2.1	24.5	98.3
$Zn_{0.1}Ti$-HZ5(30)	23.8	77.4	16.1	2.8	3.7	24.4	94.9
$Zn_{0.3}Ti$-HZ5(30)	22.4	76.0	18.2	2.1	3.7	25.1	95.1
$Zn_{0.5}Ti$-HZ5(30)	16.8	80.4	11.0	3.6	5.0	23.9	96.4
$Zn_{1.0}Ti$-HZ5(30)	15.2	79.2	11.4	5.0	4.4	24.5	96.7
ZnO-HZ5(30)	13.5	81.3	6.7	5.6	6.5	24.4	97.0
HZSM-5(30)	1.3	86.8	4.7	8.3	0.2	23.1	99.7

a) Reaction conditions: temperature = 698 K, pressure = 3 MPa, H_2:CO_2= 3:1, GHSV = 9000 h^{-1}, LHSV = 1.8 h^{-1}; Phenyl ring yield = $\dfrac{\text{Phenyl ring in the product}}{\text{Phenyl ring in the reactant}}$

$= \left[\dfrac{m_{\text{effluent}}}{(1 - \text{Conv}_{\text{benz}})M_{\text{benz}} + \sum \text{Conv}_{\text{benz}} \times \text{Select } M_{\text{i}}} \right] / \dfrac{m_{\text{Feed}}}{M_{\text{benz}}}$; c) EBZ means ethylbenzene; d) PX/X means p-xylene/xylene.

Table 3 Gaseous phase compositions and conversions of CO_2[a]

Catalyst	CO_2 Conv/%	Selectivity of product/%						CO_2 efficiency/% [b]
		CO	CH_4	C_2	C_3	C_{4+}	EBZ + C_{9+}	
TiO_2-HZ5(30)	12.0	29.7	60.2	2.7	4.6	0.0	0.4	2.3
$Zn_{0.01}Ti$-HZ5(30)	23.9	31.4	47.0	3.6	7.0	0.9	1.1	9.0
$Zn_{0.1}Ti$-HZ5(30)	25.7	35.0	21.7	2.6	8.5	3.0	3.8	25.4
$Zn_{0.3}Ti$-HZ5(30)	27.5	50.0	14.1	2.5	7.1	3.9	2.9	21.4
$Zn_{0.5}Ti$-HZ5(30)	28.9	55.5	12.5	1.4	7.3	5.1	3.2	14.9
$Zn_{1.0}Ti$-HZ5(30)	30.3	59.8	5.7	1.9	9.6	7.3	2.93	12.8
ZnO-HZ5(30)	21.9	62.9	3.1	1.1	8.9	4.8	4.7	14.6

a) Reaction conditions were the same as those in Table 2;
b) CO_2 efficiency = $\dfrac{CO_2 \text{ transferred into toluene and xylene}}{\text{converted } CO_2} = \dfrac{\text{Feed}_{\text{benz}} \ \text{Conv}_{\text{benz}}(1 \times \text{Select}_{\text{tol}} + 2 \times \text{Select}_{\text{xyl}})}{\text{Feed}_{CO_2} \times \text{Conv}_{CO_2}}$.

was possibly owing to that ZnO acted as active sites for RWGS [47]. To quantitively measure how many carbon atoms in CO_2 can be used to produce toluene and xylene, the parameter of 'CO$_2$ efficiency' was introduced as shown in Table 3. $Zn_{0.1}Ti$-HZ5(30) possessing the highest CO_2 conversion also showed the highest CO_2 efficiency, while CO_2 was mainly transformed to byproducts like CO and methane, which led CO_2 efficiency less than 20% in other samples.

To analyze the structure-performance relationships of various Zn/Ti oxides, catalytic results and OVs were analyzed on correlation as shown in Fig. 7. It can be seen that conversions of benzene and CO_2 increased almost linearly with OVs. As previously reported, OVs were responsible for the adsorption and activation of CO_2 [14,31], thus it was reasonable to attribute the promotion of conversion to the enhancement of OVs. The interaction between Zn and Ti was adjusted by changing Zn/Ti ratios, resulting in transformation of Zn/Ti oxide crystals from brookite to anatase. Compared with brookite, anatase

possessed more OVs and OVs were intensified by doping with proper amount of ZnO, improving CO_2 adsorption. Besides, ZnO as active sites also offered hetero-dissociated hydrogen that was used for hydrogenation of CO_2. However, ZnO also act as catalysts for RWGS reactions, so too many ZnO strongly effected the main reaction. As a result, $Zn_{0.1}Ti$ was the most active sample owing to the highest OVs content and proper surface-enriched ZnO, which rose from its unique structure and proper compositions, as evidenced in XRD, XPS and Raman spectrums.

3.2.3 Effects of Si/Al ratios

Acidity of HZSM-5 has a great relationship with the ratio of silicon to aluminum. The impacts of Si/Al ratios on ABCH reaction were investigated using combination of different HZSM-5 and $Zn_{0.1}Ti$. Table 4 and Table 5 show the compositions of gaseous state and liquid state products, respectively. According to the evaluation results, it can be clearly found that HZSM-5 with low Si/Al ratios showed
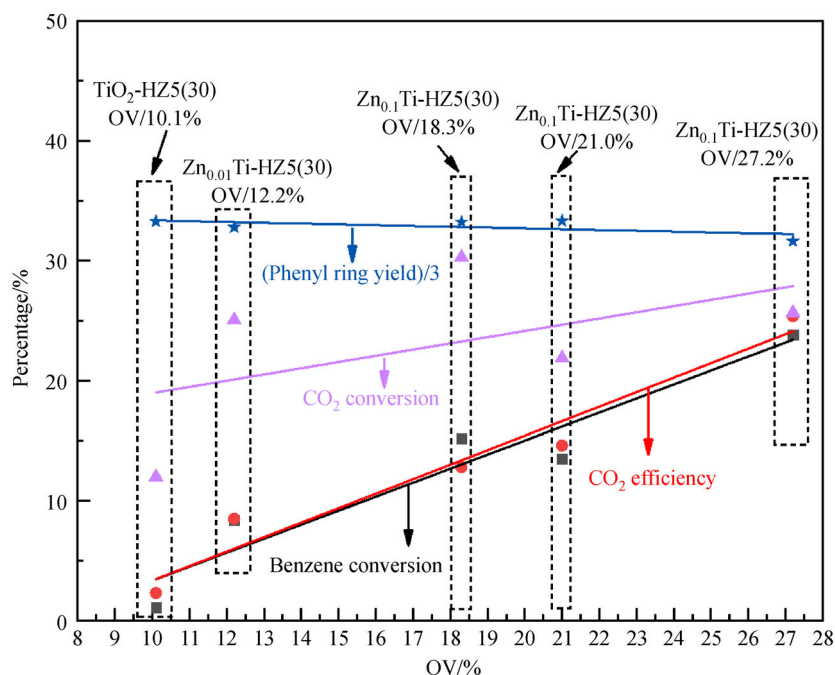
Fig. 7 Relation diagrams of OV and catalytic activity.

Table 4 Distribution and selectivity of liquid alkylation products of catalysts with different Si/Al ratios [a]

Catalyst	Conversion/%	Selectivity/%					Phenyl ring yield/% [b]
	Benzene	Toluene	Xylene	EBZ	C_{9+}	PX/X	
$Zn_{0.1}Ti-HZ5(13.5)$	28.7	72.9	17.6	4.6	4.9	25.0	93.6
$Zn_{0.1}Ti-HZ5(30)$	23.8	77.4	16.1	2.8	3.7	24.4	94.9
$Zn_{0.1}Ti-HZ5(100)$	8.6	90.7	7.7	0.6	1.0	26.7	98.3

a) Reaction conditions were the same as those in Table 2; b) the calculation method of phenyl ring yield was the same as that in Table 2.

Table 5 Gaseous phase compositions and conversions of CO_2 [a]

| Catalyst	CO_2 Conv./%	Selectivity of products/%						CO_2 efficiency [b]/%
		CO	CH_4	C_2	C_3	C_{4+}	EBZ + C_{9+}	
$Zn_{0.1}Ti-HZ5(13.5)$	29.9	39.6	10.1	2.9	11.5	4.2	5.8	25.9
$Zn_{0.1}Ti-HZ5(30)$	25.7	35	21.7	2.6	8.5	3.0	3.8	25.4
$Zn_{0.1}Ti-HZ5(100)$	25.3	55.3	34.5	0.5	0.2	0.1	0.4	9

a) Reaction conditions were the same as those in Table 2; b) the calculation method of CO_2 efficiency was the same as that in Table 3.

better catalytic activities, both CO_2 and benzene conversions via $Zn_{0.1}Ti-HZ5(13.5)$ were higher than another two samples employing $Zn_{0.1}Ti-HZ5(30)$ or $Zn_{0.1}Ti-HZ5(100)$. In the liquid products, the toluene and xylene selectivity of $Zn_{0.1}Ti-HZ5(13.5)$ dropped with more ethylbenzene and C_{9+} as side products. However, in the gas phase less CO and methane were detected leading to a higher CO_2 efficiency. As hypothesized, methanol might be the intermediate, and the timely consumption of methanol via acid sites could help to circumvent the thermodynamic limit, or else CO_2 could be transformed into other chemicals, resulting in decline of CO_2 efficiency. HZSM-5 with lower Si/Al ratio has been proved to have more acid sites via NH_3-TPD, as a result, the intermediates were more easily to be consumed and more CO_2 could be converted or utilized [48].

3.2.4 Stability tests

The time-on-stream of $Zn_{0.1}Ti-HZ5(13.5)$ catalyst was investigated and the results are displayed in Fig. 8. No obvious changes in conversion or selectivity have been
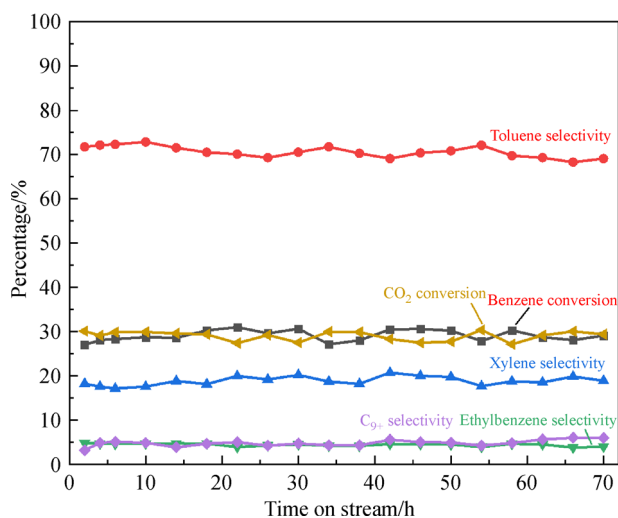
Fig. 8 Stability of $Zn_{0.1}Ti$-HZ5(13.5) catalyst in ABCH reaction.

found within 70 h, indicating that the catalyst had excellent stability.

3.3 Investigation of reaction mechanism

To further explore the reaction pathways, *in-situ* IR spectroscopies were carried using $Zn_{0.1}Ti$, HZSM-5(13.5) and $Zn_{0.1}Ti$-HZ5(13.5) at 0.6 MPa and 573 K (Fig. 9 and Figs. S(6,7), cf. ESM). As shown in Fig. S6(a1,a2) and Fig. S6(b1,b2), characteristic peaks standing for methoxy (2827, 2870, 2931, 2959 and 2980 cm^{-1}) [27,31,43,46] and formate (1360, 1582 and 1620 cm^{-1}) have been resolved when CO_2/H_2 was fed into $Zn_{0.1}Ti$ under atmosphere pressure [5,32]. After the feeding of CO_2/H_2, argon saturated by benzene was introduced into $Zn_{0.1}Ti$. In Fig. S6(b1,b2), it can be seen that IR peaks representing benzene (1400–1500, 1800–2000, 2890 and 3000–3100 cm^{-1}) [9,49] appeared and those peaks of formate and carbonate were reserved. However, no peaks were found
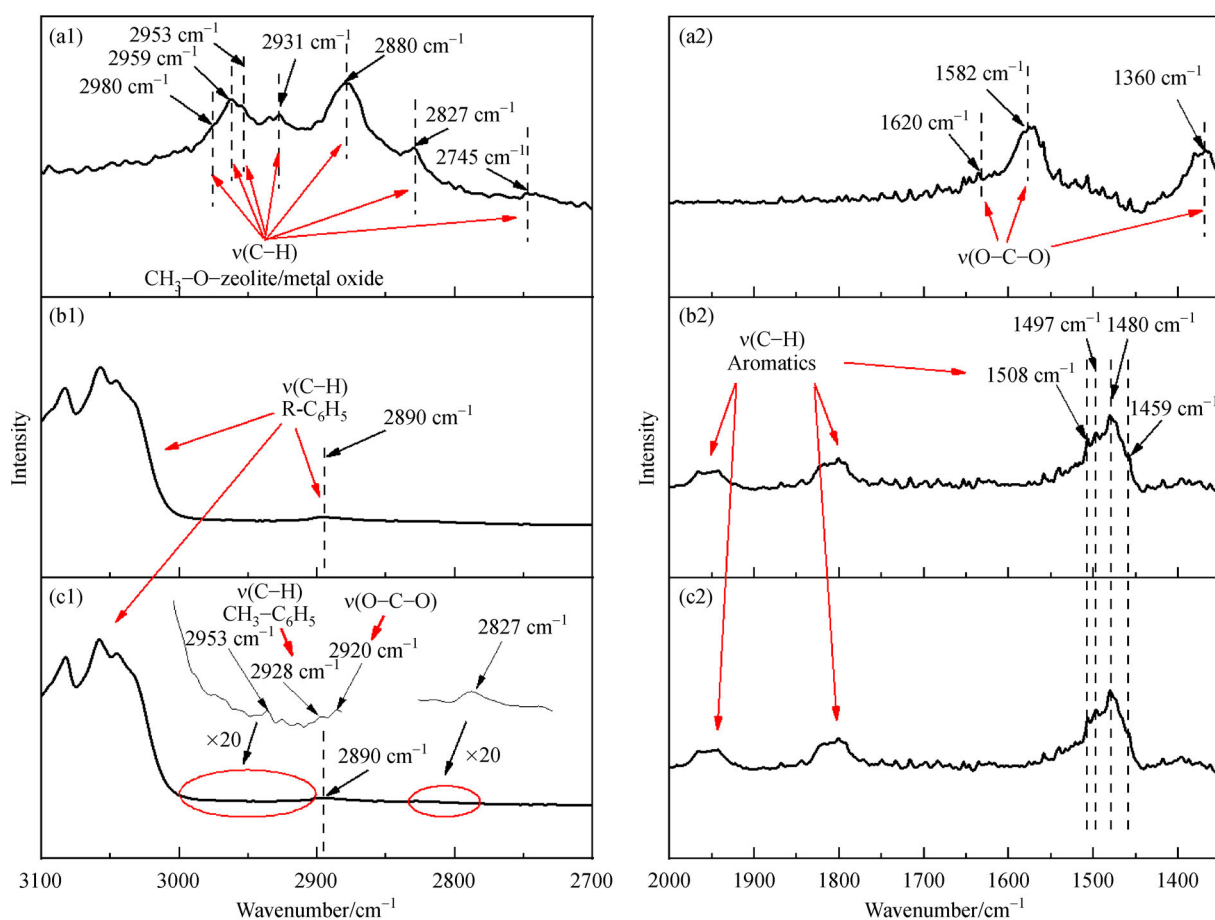
Fig. 9 *In-situ* IR spectra of $Zn_{0.1}Ti$-HZ5(13.5) catalyst recorded at 598 K under 0.6 MPa: (a1,a2) The mixture of carbon dioxide and hydrogen (10 mL/min, H_2:CO_2= 3:1) was introduced into the *in-situ* pool (598 K and 0.6 MPa) containing an unreacted catalyst for 30 min. Afterward, the *in-situ* pool was swept by argon gas for 10 min; (b1,b2) after above experiment, benzene vapor was carried by argon (10 mL/min) into the *in-situ* pool, measured via IR spectra; (c1,c2) mixture gas of carbon dioxide and hydrogen carried benzene vapors into the *in-situ* pool under the condition and subsequent steps which were the same as experiments (a1,a2) and (b1,b2).

when either CO_2/H_2 or benzene was injected into HZSM-5, as shown in Fig. S6(c1,c2) and Fig. S6(d1,d2), which was consistent with the fact that sole HZSM-5 was invalid for ABCH reaction (Table 2). These results indicate that carbon dioxide and hydrogen formed formates and methoxides on metal oxides rather than on HZSM-5, meanwhile, mono-functional catalyst as Zn/Ti oxides or HZSM-5 alone cannot achieve conversion of benzene.

In order to examine the formation of methoxy and formate species on $Zn_{0.1}Ti$ oxide, CO_2 and H_2 were pumped into the *in-situ* pool in sequence. Carbonate and bicarbonate species (1550 and 1337 cm^{-1}) [33] were mainly observed on $Zn_{0.1}Ti$ by contacting with CO_2 (Fig. S7), nonetheless vibration peaks of formate and methoxide species have not been found. Then, H_2 instead of CO_2 was introduced into the *in-situ* pool, the as-observed peaks in the former step changed significantly, along with the appearance of formate species at 1360, 1582 and 1620 cm^{-1}. Prolonging the contact time with H_2, formate and carbonate species decreased gradually, while the peaks of methoxy species increase obviously, implying the formate and carbonate species were probably transformed into methoxy species.

In addition, HZSM-5 coupled with $Zn_{0.1}Ti$ was placed in CO_2/H_2 to verify the reaction route of benzene (Fig. 9). At first, methoxy peaks and formate peaks gradually emerged. On switching the gas into benzene saturated argon, methoxy and formate species weakened and finally vanished thoroughly, it illustrated that formate and methoxy have been consumed by benzene. There was no characteristic peak of substituted benzene in the process,

which may be owing to the insufficient amounts of substituted benzenes. To confirm the existence of substituent benzene, benzene saturated CO_2/H_2 was introduced into the cell. The spectrum (Fig. 9(c1)) shows the vibration peaks representing methyl-benzene at 2928 cm^{-1} [9,49], demonstrating the generation of alkyl-benzene. This was also confirmed by the catalytic data in Table 2.

The reaction pathway (Fig. 10) would be manifested in the results of *in-situ* IR spectroscopies. Firstly, carbon dioxide was adsorbed on the OVs of the metal oxide surface, forming carbonate species [31–33]. With dissociation of H_2 (activated on ZnO), carbonate was hydrogenated into formate species and further to methoxy species. Methoxy was an important precursor for methanol [26,50], so it can be assumed that methanol was synthesized on Zn/Ti oxide, then it was rapidly transferred onto HZSM-5 zeolite and protonated into another type of methoxy group connecting with the zeolite framework. Methoxy species on the zeolite were rather active and they reacted with benzene readily when benzene was available [17,22,25]. During the whole process, methanol as the key intermediate was strictly limited by thermodynamics and it will be transformed into methoxy groups quickly then consumed by benzene, so the content of methanol was kept at a low level. This also explains why no methanol was detected, but the functional groups like formate, carbonate and methoxy can be found. Overall, ABCH required a synergistic effect of metal oxides and molecular sieves, metal oxides provided OVs and ZnO for the activation of CO_2/H_2, while the molecular sieves were responsible for the activation of benzene.
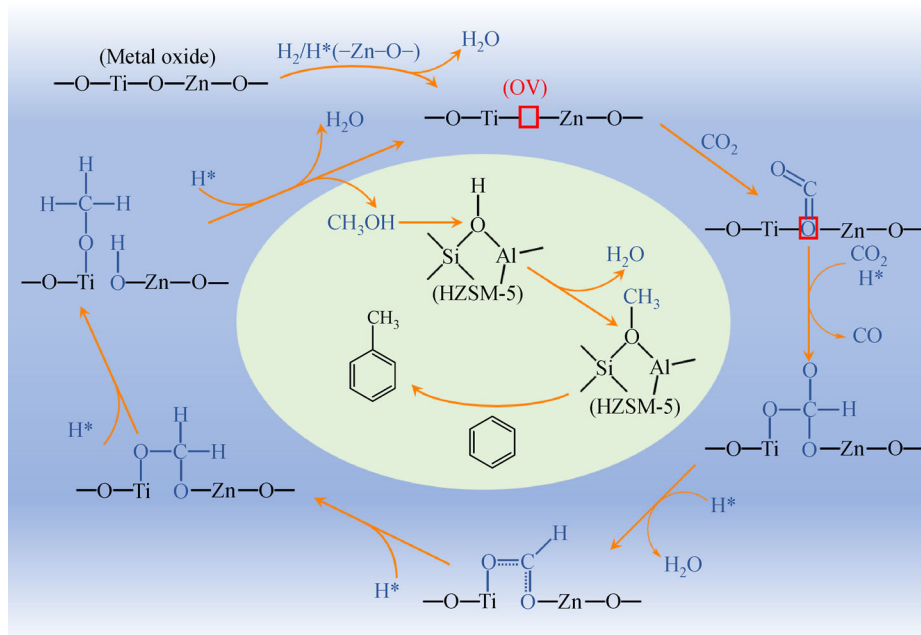
Fig. 10 Reaction mechanism for the ABCH on the Zn/Ti-HZSM-5 catalyst.

4 Conclusions

High value-added products such as toluene and xylene were obtained via ABCH reaction in a fixed bed reactor, and a series of low-cost bifunctional Zn/Ti-HZSM-5 catalysts were developed. The optimal conditions for ABCH reaction were: 698 K, 3 MPa, $H_2:CO_2 = 3:1$, GHSV $= 9000$ h^{-1}, LHSV $= 1.8$ h^{-1}. Benzene conversion and total selectivity of toluene and xylene can reach 28.7% and 29.9%, respectively at the optimized conditions. $Zn_{0.1}Ti$-HZ5(13.5) was proved to be the most active catalyst as a result of the anatase phase and a proper quantity of ZnO on the surface, which offered abounding OVs and suitable hydrogenation capacity. Simultaneously, the HZSM-5 with low Si/Al ratios (Si/Al = 13.5) showed more acidic sites, in which unstable intermediates can be reacted readily. These features of metal oxides and zeolites guarantee the reaction activity and high-selectivity. Besides, the reaction mechanism was studied via *in-situ* infra-red spectroscopy. *In-situ* spectrums revealed that CO_2 was adsorbed on Zn/Ti oxides and transformed to carbonate or decarbonate first. Afterwards, these intermediates were progressively converted to formate and methoxy groups by hydrogenation of dissociated H_2, and finally changed into methanol. At last, methanol immigrated to zeolites and reacts with benzene to generate alkylates. These findings provide a novel route for the efficient utilization of carbon dioxide and preparation of high-value aromatic hydrocarbons, which also contributes to global environmental protection.

Electronic Supplementary Material Supplementary material is available in the online version of this article at http://dx.doi.org/10.1007/s11705-021-2045-y and is accessible for authorized users.

References

1. Cored J, Garcia-Ortiz A, Iborra S, Climent M, Liu L, Chuang C, Chan T, Escudero C, Concepcion P, Corma A. ydrothermal synthesis of ruthenium nanoparticles with a metallic core and a ruthenium carbide shell for low-temperature activation of CO_2 to methane. Journal of the American Chemical Society, 2019, 141(49): 19304–19311

2. Ye R, Ding J, Gong W, Argyle M, Zhong Q, Wang Y, Russell C, Xu Z, Russell A, Li Q, Fan M, Yao Y G. CO_2 hydrogenation to high-value products via heterogeneous catalysis. Nature Communications, 2019, 10(1): 1–15

3. Dixneuf P. A bridge from CO_2 to methanol. Nature Chemistry, 2011, 3(8): 578–579

4. Li Z, Qu Y, Wang J, Liu H, Li M, Miao S, Li C. Highly selective conversion of carbon dioxide to aromatics over tandem catalysts. Joule, 2019, 3(2): 570–583

5. Ni Y, Chen Z, Fu Y, Liu Y, Zhu W, Liu Z. Selective conversion of CO_2 and H_2 into aromatics. Nature Communications, 2018, 9(1): 1–7

6. Gao P, Li S, Bu X, Dang S, Liu Z, Wang H, Zhong L, Qiu M, Yang C, Cai J, Wei W, Sun Y. Direct conversion of CO_2 into liquid fuels with high selectivity over a bifunctional catalyst. Nature Chemistry, 2017, 9(10): 1019–1024

7. Christensen C, Johannsen K, Schmidt I, Christensen C. Catalytic benzene alkylation over mesoporous zeolite single crystals: improving activity and selectivity with a new family of porous materials. Journal of the American Chemical Society, 2003, 125 (44): 13370–13371

8. Mikkelsen Ø, Rønning P, Kolboe S. Use of isotopic labeling for mechanistic studies of the methanol-to-hydrocarbons reaction. Microporous and Mesoporous Materials, 2000, 40(1): 95–113

9. Yang F, Zhong J, Liu X, Zhu X. A novel catalytic alkylation process of syngas with benzene over the cerium modified platinum supported on HZSM-5 zeolite. Applied Energy, 2018, 226: 22–30

10. Saeidi S, Amin N, Rahimpour M. Hydrogenation of CO_2 to value-added products-a review and potential future developments. Journal of CO_2 Utilization, 2014, 5: 66–81

11. Ting K, Kamakura H, Poly S, Toyao T, Siddiki S, Maeno Z, Matsushita K, Shimizu K. Catalytic methylation of aromatic hydrocarbons using CO_2/H_2 over Re/TiO_2 and H-MOR catalysts. ChemCatChem, 2020, 12(8): 1–7

12. Zeng M, Li Y, Mao M, Bai J, Ren L, Zhao X. Synergetic effect between photocatalysis on TiO_2 and thermocatalysis on CeO_2 for gas-phase oxidation of benzene on TiO_2/CeO_2 nanocomposites. ACS Catalysis, 2015, 5(6): 3278–3286

13. Li Z, Wnetrzak R, Kwapinski W, Leahy J. Synthesis and characterization of sulfated TiO_2 nanorods and ZrO_2/TiO_2 nano-composites for the esterification of biobased organic acid. ACS Applied Materials & Interfaces, 2012, 4(9): 4499–4505

14. Cheng K, Zhou W, Kang J, He S, Shi S, Zhang Q, Pan Y, Wen W, Wang Y. Bifunctional catalysts for one-step conversion of syngas into aromatics with excellent selectivity and stability. Chem, 2017, 3 (2): 334–347

15. Wang J, Li G, Li Z, Tang C, Feng Z, An H, Liu H, Liu T, Li C. A highly selective and stable $ZnO-ZrO_2$ solid solution catalyst for CO_2 hydrogenation to methanol. Science Advances, 2017, 3(10): e1701290

16. Arin J, Thongtem S, Phuruangrat A, Thongtem T. Characterization of $ZnO-TiO_2$ and zinc titanate nanoparticles synthesized by hydrothermal process. Research on Chemical Intermediates, 2016, 43(5): 3183–3195

17. Qu Y, Zhou W, Ren Z, Wang G, Jiang B, Fu H. Facile synthesis of porous $Zn_2Ti_3O_8$ nanorods for photocatalytic overall water splitting. ChemCatChem, 2014, 6(8): 2258–2262

18. Wang C, Hwang W, Ko H, Hsi C, Chang K, Wang M. Phase transformation and microstructure of $Zn_2Ti_3O_8$ nanocrystallite powders prepared using the hydrothermal process. Metallurgical and Materials Transactions. A, Physical Metallurgy and Materials Science, 2013, 45(1): 250–260

19. Kruse N, Chenakin S. XPS characterization of Au/TiO_2 catalysts: binding energy assessment and irradiation effects. Applied Catalysis A, General, 2011, 391(1-2): 367–376

20. Biesinger M, Lau L, Gerson A, Smart R. Resolving surface chemical states in XPS analysis of first row transition metals, oxides and hydroxides: Sc, Ti, V, Cu and Zn. Applied Surface Science, 2010, 257(3): 887–898

21. Chenakin S, Kruse N. Combining XPS and ToF-SIMS for assessing the CO oxidation activity of Au/TiO_2 catalysts. Journal of Catalysis, 2018, 358: 224–236

22. Xin X, Xu T, Yin J, Wang L, Wang C. Management on the location and concentration of Ti^{3+} in anatase TiO_2 for defects-induced visible-light photocatalysis. Applied Catalysis B: Environmental, 2015, 176-177: 354–362

23. Chai Y, Li L, Lu J, Li D, Shen J, Zhang Y, Liang J, Wang X. Germanium-substituted Zn_2TiO_4 solid solution photocatalyst for conversion of CO_2 into fuels. Journal of Catalysis, 2019, 371: 144–152

24. Xiao F. Construction of highly ordered ZnO-TiO_2 nanotube arrays (ZnO/TNTs) heterostructure for photocatalytic application. ACS Applied Materials & Interfaces, 2012, 4(12): 7055–7063

25. Katea S, Broqvist P, Kullgren J, Hemmer E, Westin G. Fast, low-cost synthesis of ZnO: Eu nanosponges and the nature of Ln doping in ZnO. Inorganic Chemistry, 2020, 59(11): 7584–7602

26. He Z, Que W, Chen J, He Y, Wang G. Surface chemical analysis on the carbon-doped mesoporous TiO_2 photocatalysts after post-thermal treatment: XPS and FTIR characterization. Journal of Physics and Chemistry of Solids, 2013, 74(7): 924–928

27. Yang F, Fang Y, Liu X, Li X, Muir D, Maclennan A, Zhu X. One-step alkylation of benzene with syngas over non-noble catalysts mixed with modified HZSM-5. Industrial & Engineering Chemistry Research, 2019, 58(31): 13879–13888

28. Wagata H, Sakakibara K, Kawashima K, Hojamberdiev M, Yubuta K, Teshima K. Alkali metal chloride flux growth of ilmenite-type $ZnTiO_3$ and subsequent nitrogen doping for visible-light-driven water oxidation catalysis. ACS Applied Energy Materials, 2019, 2(11): 7762–7771

29. Wang M, Han J, Hu Y, Guo R, Yin Y. Carbon-incorporated NiO/TiO_2 mesoporous shells with p-n heterojunctions for efficient visible light photocatalysis. ACS Applied Materials & Interfaces, 2016, 8(43): 29511–29521

30. Kam R, Selomulya C, Amal R, Scott J. The influence of La-doping on the activity and stability of Cu/ZnO catalyst for the low-temperature water-gas shift reaction. Journal of Catalysis, 2010, 273(1): 73–81

31. Liu X, Wang M, Zhou C, Zhou W, Cheng K, Kang J, Zhang Q, Deng W, Wang Y. Selective transformation of carbon dioxide into lower olefins with a bifunctional catalyst composed of $ZnGa_2O_4$ and SAPO-34. Chemical Communications, 2018, 54(2): 140–143

32. Ye J, Liu C, Mei D, Ge Q. Active oxygen vacancy site for methanol synthesis from CO_2 hydrogenation on In_2O_3(110): a DFT study. ACS Catalysis, 2013, 3(6): 1296–1306

33. Zhou C, Shi J, Zhou W, Cheng K, Zhang Q, Kang J, Wang Y. Highly active ZnO-ZrO_2 aerogels integrated with H-ZSM-5 for aromatics synthesis from carbon dioxide. ACS Catalysis, 2019, 10(1): 302–310

34. Hu W, Li L, Li G, Tang C, Sun L. High-quality brookite TiO_2 flowers: synthesis, characterization, and dielectric performance.

Crystal Growth & Design, 2009, 9(8): 3676–3682

35. Pal S, Laera A, Licciulli A, Catalano M, Taurino A. Biphase TiO_2 microspheres with enhanced photocatalytic activity. Industrial & Engineering Chemistry Research, 2014, 53(19): 7931–7938

36. Wang H, Chen L, Su W, Chung J, Hwang B. Effect of the compact TiO_2 layer on charge transfer between N_3 dyes and TiO_2 investigated by Raman spectroscopy. Journal of Physical Chemistry C, 2010, 114(7): 3185–3189

37. Chong S, Suresh N, Xia J, Al-Salim N, Idriss H. TiO_2 nanobelts/CdSSe quantum dots nanocomposite. Journal of Physical Chemistry C, 2007, 111(28): 10389–10393

38. Dong J, Zhang X, You J, Cai P, Yin Z, An Q, Ma X, Jin P, Wang Z, Chu P. Effects of hydrogen plasma treatment on the electrical and optical properties of ZnO films: identification of hydrogen donors in ZnO. ACS Applied Materials & Interfaces, 2010, 2(6): 1780–1784

39. Song H, Laudenschleger D, Carey J, Ruland H, Nolan M, Muhler M. Spinel-structured $ZnCr_2O_4$ with wxcess Zn is the active ZnO/Cr_2O_3 catalyst for high-temperature methanol synthesis. ACS Catalysis, 2017, 7(11): 7610–7622

40. Zheng S. On the enhanced para-selectivity of HZSM-5 modified by antimony oxide. Journal of Catalysis, 2003, 219(2): 310–319

41. Bai Y, Yang F, Liu X, Liu C, Zhu X. Performance of bifunctional ZnZr/ZSM-5 catalysts in the alkylation of benzene with syngas. Catalysis Letters, 2018, 148(12): 3618–3627

42. Zhang P, Tan L, Yang G, Tsubaki N. One-pass selective conversion of syngas to para-xylene. Chemical Science (Cambridge), 2017, 8(12): 7941–7946

43. Bahruji H, Bowker M, Hutchings G, Dimitratos N, Wells P, Gibson E, Jones W, Brookes C, Morgan D, Lalev G. Pd/ZnO catalysts for direct CO_2 hydrogenation to methanol. Journal of Catalysis, 2016, 343: 133–146

44. Choi E, Lee Y, Lee D, Moon D, Lee K. Hydrogenation of CO_2 to methanol over Pd-Cu/CeO_2 catalysts. Molecular Catalysis, 2017, 434: 146–153

45. Lyu J, Hu H, Tait C, Rui J, Lou C, Wang Q, Han W, Zhang Q, Pan Z, Li X. Benzene alkylation with methanol over phosphate modified hierarchical porous ZSM-5 with tailored acidity. Chinese Journal of Chemical Engineering, 2017, 25(9): 1187–1194

46. Svelle S, Visur M, Olsbye U, Bjørgen M. Mechanistic aspects of the zeolite catalyzed methylation of alkenes and aromatics with methanol: a review. Topics in Catalysis, 2011, 54(13-15): 897–906

47. Murthy P, Wang Z, Wang L, Zhao J, Wang Z, Liang W, Huang J. Improved CO_2 hydrogenation on Ni-ZnO/MCM-41 catalysts with cooperative Ni and ZnO sites. Energy & Fuels, 2020, 34(12): 16320–16329

48. Wang Q, Wang L, Wang H, Li Z, Zhang X, Zhang S, Zhou K. Effect of SiO_2/Al_2O_3 ratio on the conversion of methanol to olefins over molecular sieve catalysts. Frontiers of Chemical Science and Engineering, 2011, 5(1): 79–88

49. Zuo J, Chen W, Liu J, Duan X, Ye L, Yuan Y. Selective methylation of toluene using CO_2 and H_2 to para-xylene. Science Advances, 2020, 6(34): eaba5433

50. Tobin C, Ian A, Alexis T. *In situ* infrared study of methanol synthesis from CO_2/H_2 on titania and zirconia promoted Cu/SiO_2. Journal of Catalysis, 1999, 184(1): 144–156